Desalination and Water Treatment
www.deswater.com

doi: 10.5004/dwt.2017.21539

97 (2017) 272–284
November

Preparation of NH_2-SH-GO/MWCNTs composite for simultaneous removal of Pb(II), Zn(II) and phenol from aqueous solution

Lili Jiang[a,b,*], Chuantong Li[a], Haitao Yu[c], Zongshu Zou[b], Fengman Shen[b], Xingang Hou[a]

[a]*School of Material Science and Technology, Lanzhou University of Technology, Langongping Road, Lanzhou 730050, Gansu Province, P.R. China, Tel./Fax: +86 24 83681545; email: jianglili2002@163.com (L. Jiang), Tel. +86 931 2976378; Fax: +86 931 2976702; emails: L272395355@163.com (C. Li), houxg1958@163.com (X. Hou)*
[b]*School of Metallurgy, Northeastern University, No. 3-11, Wenhua Road, Heping District, Shenyang, Liaoning Province, P.R. China, Tel./Fax: +86 24 83681545; emails: zouzs@mail.neu.edu.cn (Z. Zou), shenfm@mail.neu.edu.cn (F. Shen).*
[c]*Department of Medical Laboratory, The First Hospital of Lanzhou University, No. 1, Donggang Road, Chengguan District, Lanzhou 730000, Gansu Province, P.R. China, Tel. +86 931 8626421; Fax: +86 931 8619797; email: yuhaitao7707@163.com*

Received 12 May 2017; Accepted 4 October 2017

ABSTRACT

In the present work, NH_2-SH-GO/MWCNTs that graphene oxide (GO) and multiwalled carbon nanotubes (MWCNTs) were chemically modified with amino and sulfydryl groups, were synthesized by a simple process for simultaneous adsorption of pollutants, such as Pb^{2+}, Zn^{2+} and phenol in water solution. The structure of composite (NH_2-SH-GO/MWCNTs) was analyzed by transmission electron microscopy, scanning electron microscopy, Fourier transform infrared spectroscopy, thermogravimetric analysis, Raman spectrum, X-ray diffraction and X-ray photoelectron spectroscopy. Brunauer–Emmett–Teller surface areas and pore diameter were studied by nitrogen adsorption–desorption isotherms. Experimental conditions affecting adsorption process, such as pH, initial ion concentrations and adsorbent dosages, were studied. Adsorption process of metal ions and phenol was evaluated by Langmuir and Freundlich isotherm models. Pseudo-first-order and pseudo-second-order kinetic models were tested for fitting the adsorption data. The optimum conditions, specified as 25 mg/L of adsorbent, 10 mg/L of adsorbate at pH 5 and time of 60 min, led to the achievement of a high adsorption capacity. The maximum adsorption capacity of NH_2-SH-GO/MWCNTs was 125.8, 98.6 and 23.8 mg/g for Pb^{2+}, Zn^{2+} and phenol, respectively. The results of adsorption isotherm and kinetics showed a good fit to Freundlich isotherm model and pseudo-second-order kinetic model, respectively. Thermodynamic parameters, such as ΔG^{θ}, ΔH^{θ} and ΔS^{θ}, were calculated. The thermodynamics results indicated the adsorption process was spontaneous and endothermic. The adsorption performance of adsorbent indicated the feasibility of applying for industrial purposes.

Keywords: Adsorption; Graphene oxide; Metal ions; Phenol; MWCNTs

1. Introduction

Since the industrial revolution, water pollution has become a critical environmental and economic issue in the world [1]. Industrial sewage contains many pollutants, such as lead, zinc ions and phenol. Among these pollutants, lead and zinc ions can enter into the environment and cause anemia and peripheral neuritis to the body because of their toxicity and bioaccumulation in the bodies [2]. Moreover, phenol is also found to be highly poisonous to human bodies. For instance, phenol can damage the function of liver and kidney in fauna [3].

Several methods have been applied for the removal of metal ions and phenol from aqueous solution. Totally speaking, traditional methods, such as sulfide precipitation [4], ion exchange [5], alum treatment [6], membrane separation,

* Corresponding author.

reverse osmosis, ion coagulation [7] and so on, were applied. However, these traditional techniques are wasting time and separation becomes a difficult issue due to small size of ions. Furthermore, these disadvantages, such as procedural complexity and high operating cost, must be solved [8]. Among these methods, adsorption is one of the most popular and widely used techniques for cleansing of pollution, and shows a high availability and economic superiority [9].

Graphene was discovered by Geim and Novoselov [10] and carbon nanotubes (CNTs) were found by Lijima [11]. Since the finding, graphene and CNTs play an important role in many domains. In recent years, graphene oxide (GO) and CNTs have been developed to remove metal ions from aqueous solutions and they are also promising materials because of their unique electrical, mechanical, thermal, optical and chemical properties [12,13]. There are various functional groups on the GO sheets and CNTs, such as hydroxyl and carboxyl groups, which allow GO and CNTs to be functionalized or be hybridized with other materials to form composite. It is well known that GO and CNTs have large surface areas which can adsorb pollutants from water solution [14–18]. The adsorption capability of GO and multiwalled carbon nanotubes (MWCNTs) relates to functional groups, which attach to surfaces and provide strongly active sites [19,20]. Many researchers had reported a lot of surface modification strategies, such as magnetic graphene nanomaterials [21], amino-modified [22] and sulfydryl-modified [23] MWCNTs. Zhang et al. [24] developed a novel method for amine functionalized CNTs via combination of mussel inspired chemistry and Michael addition reaction. The results indicated that the adsorption capacity was much improved as compared with pristine CNTs [24]. Zhang et al. [25] synthesized water-soluble magnetic graphene nanocomposites via a copper catalyzed azide–alkyne cycloaddition reaction and used them as nanoadsorbents for recyclable removal of Cu^{2+}, Cd^{2+} and Pb^{2+} from aqueous solution. Wang et al. [26] synthesized a magnetic graphene–CNT composite material to adsorb methylene blue from aqueous solution. The results showed that the maximum adsorption capacity of the samples was up to 65.79 mg/g, which was almost equal to the sum of magnetic graphene and magnetic MWCNTs [26]. To authors' knowledge, there are few reports that applying amino and sulfydryl groups to modify GO/MWCNTs composite, and they have not been used as adsorbent to removal of metal ions and phenol.

The main objective of the present study was to synthesize NH_2-SH-GO/MWCNTs composite and investigate their adsorption capacity for metal ions and phenol from aqueous solution. In this study, synthesized adsorbents were studied by Fourier transform infrared spectroscopy (FTIR), Fourier transform Raman spectrometry, thermogravimetric analysis (TGA), transmission electron microscopy (TEM), scanning electron microscopy (SEM), X-ray diffraction (XRD), X-ray photoelectron spectroscopy (XPS) and nitrogen adsorption–desorption isotherm. Adsorption experiments with Pb^{2+}, Zn^{2+} and phenol from aqueous solution were performed. The effects of pH value, contact time, initial concentrations and temperature on adsorption capacity of NH_2-SH-GO/MWCNTs were investigated. The adsorption data were fitted with Langmuir and Freundlich isotherm models. The enthalpy, entropy and Gibbs free energy was also determined from the experimental data.

2. Experimental methods

2.1. Materials and chemicals

MWCNTs were purchased from Shenzhen Nanotech Port Co., Ltd. (China). According to the manufacturer, the physicochemical properties of MWCNTs were listed in Table 1. Natural flaky graphite (1,500 mesh) was purchased from Qingdao Tianshengda Graphite Co., Ltd. (China). Ultrapure water was used for preparation of solution. H_2SO_4, HNO_3 and acetone (purity > 99.5%) were purchased from Big Alum Chemical Reagent Factory (China). 3-Mercaptopropyl trimethoxysilane (MPTS, purity > 98%) was purchased from Shanghai Yuanye Biological Technology Co., Ltd. (China). $KMnO_4$, $NaNO_3$, $Pb(NO_3)_2$, $Zn(NO_3)_2$ and phenol were purchased from Tianjin Fu Rui Technology Co., Ltd. (China). All the chemicals were of analytical grade without further purification.

2.2. Characterization instrument

The microstructures of samples were observed with TEM (JEM-2010, operating at 200 kV) and SEM (JSM-6700F, operating at 0.5–30 kV). The adsorbent was determined by FTIR analysis (Nexus-870). All the samples were prepared by mixing spectroscopic grade KBr with NH_2-SH-GO/MWCNTs or GO/MWCNTs and they were analyzed in the 4,000–400 cm^{-1} range with a resolution of 2 cm^{-1}. Fourier transform Raman spectroscopy (RFS100/S), TGA analysis (temperature range of 100°C –800°C and heating rate of 10°C/min), XRD (Rigaku D/max-2400, operating at 60 kV), XPS (Escalab 250Xi with a maximum resolution of 400,000 cps, Al Kα radiation) were applied to analyze these materials. The results of XPS were analyzed with XPS peak software and surface atomic percentages were calculated from the corresponding peak areas. Specific surface area and porosity were measured using ASAP-2010 (Micromeritics Co., USA). Metal ion concentrations were analyzed with an atomic absorption spectrophotometer (HITACHI Z-5000), and phenol concentrations were determined by ultraviolet and visible spectrophotometer (Shanghai Precision Scientific Instrument Co., Ltd., UV-1000). A temperature controlled shaker was used for shaking aqueous solution containing metal ions and phenol. Water bath kettle (HHS2) was used for maintaining temperature of the aqueous solution. All the experimental water was produced by the ultrapure water system (Ulupure, UPD-I-20T). The pH value of the solution was measured by pH meter (PHSJ-3F).

2.3. Preparation of oxidized MWCNTs

Original MWCNTs (2 g) were placed in a three-necked bottle with 60 mL concentrated sulfuric acid and 20 mL

Table 1
Physicochemical properties of MWCNTs

Physicochemical properties	Value
Diameter, nm	10–20
Length, μm	<2
Purity, %	>97
Ash, %	<3
Special surface area, m^2/g	100–160

concentrated nitric acid to remove impurities and hemispherical caps. Then, the mixture was ultrasonically stirred in a water bath kettle for 3 h at 60°C. The suspensions were filtrated, rinsed with deionized water until pH value reached 7, followed by drying in a vacuum oven at 80°C for 12 h. The obtained product was oxidized MWCNTs (o-MWCNTs).

2.4. Preparation of GO

GO was prepared with the modified Hummers' method [27]. Natural flaky graphite (4 g) was dispersed in a three-necked bottle containing 92 mL sulfuric acid below 5°C. Stirred the mixture below 10°C until complete dissolution, followed by slow addition of 2 g sodium nitrate and 12 g potassium permanganate, then stirred for 2.5 h. The three-necked bottle was taken out, and placed it into a water bath kettle at 35°C, then 184 mL ultrapure water was added and stirred for 30 min. Again the three-necked bottle was taken out, then allowed by placing it into the water bath kettle at 85°C, stirred for 24 min and diluted to 560 mL. Then, 40 mL hydrogen peroxides (30 wt%) was added and kept warm for 5 min where the color of the mixture changed to bright yellow. Centrifuged the product and washed with 3% hydrochloric acid for several times to remove residual metal ions until pH value of product reached 7. Finally, the product was treated by ultrasonication for 1 h, centrifuged and dried in a vacuum oven for 24 h at 60°C. The obtained products were GO.

2.5. Preparation of GO/MWCNTs

Weighted GO of 0.2 g and o-MWCNTs of 0.4 g, respectively. Then, dispersed them in 100 mL absolute alcohol and treated for 2 h with ultrasound. Place the mixture into a three-necked bottle and treated with ultrasound for 2 h. Finally, pumped and filtered with 0.45 μm filter membrane, washed with absolute alcohol for several times and the product was dried in a vacuum oven for 12 h at 60°C.

2.6. Preparation of NH_2-SH-GO/MWCNTs

GO/MWCNTs of 400 mg were dispersed into 80 mL absolute alcohol at 25°C. Then, 4 mL acetic acid and 8 mL MPTS were added to the mixture. The entire experimental process was protected under nitrogen gas while continually stirred. The reaction time was 24 h at 25°C. After the reaction, 100 mL acetone was slowly added to the reaction solution. The product was passed through filter paper and washed with ethanol and ultrapure water. The product was dried in a vacuum drying oven at 60°C for 8 h. The products were SH-GO/MWCNTs. SH-GO/MWCNTs (200 mg) were suspended into 50 mL absolute alcohol. The mixture was stirred vigorously, and then slowly reacted for 5 min after adding 10 mL hydrazine hydrate (80 wt%). Then, the solution was placed in a water bath kettle and stirred for 6 h. Subsequently, the composite was filtered and washed with ultrapure water for several times. Finally, the product was dried in a vacuum oven for 8 h at 60°C. The obtained composite was NH_2-SH-GO/MWCNTs.

2.7. Adsorption experiment

The adsorption behavior of as-prepared composite was carried out by a batch adsorption experiment, which was performed by adsorbing lead, zinc ions and phenol from aqueous solution. The effect of pH on the adsorption performance was studied at initial pH value which ranged from 2 to 9. The pH values of solution were adjusted by adding aqueous solutions of HCl or NaOH. The initial concentration of Pb^{2+}, Zn^{2+} and phenol in solution was 10 mg/L, respectively, and 2.5 mg adsorbents was in every 100 mL solution. The effect of time was studied at the time intervals of 15, 30, 60, 120, 240, 480, 720, 1,440 and 2,160 min with an initial concentration of 10 mg/L for Pb^{2+}, Zn^{2+} and phenol, respectively. Adsorbents (2.5 mg) were dispersed into 100 mL solution at pH 5. To investigate the adsorption isotherm, the initial concentration was ranged from 5 to 30 mg/L at 25°C at pH 5. The effect of temperature on the adsorption process was investigated by controlling temperature at 288, 293, 298, 303 and 308 K at pH 5 for 8 h. The liquid after adsorption was filtered with 0.45 μm filter membrane. The exact concentrations of Pb^{2+} and Zn^{2+} were determined with an atomic absorption spectrophotometer and phenol concentration was measured by ultraviolet and visible spectrophotometer.

Adsorption capacity is calculated with the following equation [28]:

$$q_e = \frac{(C_0 - C_e)V}{m} \tag{1}$$

where q_e is the adsorption capacity of adsorbent at equilibrium (mg/g), C_0 is the initial concentration of adsorbate in solution (mg/L), C_e is the concentration of adsorbate at equilibrium (mg/L), V is the volume of solution (L) and m is the weight of adsorbent (g).

The kinetics of Pb^{2+}, Zn^{2+} and phenol removed from aqueous solution by NH_2-SH-GO/MWCNTs was studied by applying pseudo-first-order and pseudo-second-order models. The equations describing the two studied models are presented as follows [29,30]:

$$\ln(q_e - q_t) = \ln q_e - k_1 t \tag{2}$$

$$\frac{1}{q_t} = \frac{1}{k_2 q_e^2} + \frac{t}{q_e} \tag{3}$$

$$h = k_2 q_e^2 \tag{4}$$

where q_e (mg/g) and q_t (mg/g) are the adsorption capacity of adsorbent at equilibrium and at time of t, respectively; k_1 is the pseudo-first-order rate constant and k_2 is the pseudo-second-order rate constant; h is the initial rate of adsorption (mg/g min), when t is nearly to zero.

Langmuir isotherm model was valid for monolayer adsorption onto the surface. Freundlich isotherm model was based on an exponential distribution of adsorption sites and energies. It was derived from multilayer adsorption and heterogeneous surface. The adsorption isotherm, such

as Langmuir and Freundlich isothermal model, is shown as follows [31,32]:

$$\frac{C_e}{q_e} = \frac{C_e}{q_{\max}} + \frac{1}{bq_{\max}} \tag{5}$$

$$\log q_e = \frac{1}{n}\log C_e + \log K_f \tag{6}$$

where q_e and C_e represent adsorption capacity at equilibrium (mg/g) and the concentration of adsorbate at equilibrium (mg/L), respectively; $q_{\max}$ is considered the maximum adsorption capacity related to the total surface and b is associated with sorption energy. In the Freundlich model, K_f represents the sorption capacity and $1/n$ is related to the energy distribution of sorption sites.

3. Results and discussion

3.1. Characterization results

Fig. 1 shows that the flow charts of preparation and adsorption experiment of NH_2-SH-GO/MWCNTs. We prepare the o-MWCNTs and GO and synthesize the composite of GO/MWCNTs. GO and MWCNTs form the composite attributing to π–π interaction in the synthetic process. To improve the adsorption capacity, we add amino and sulfydryl groups on the surface. But after adding amino groups, oxygenous functional groups of composite gradually decrease, which leads to the regional hydrophobicity [33]. And we apply the prepared adsorbent to adsorb metal ions and phenol in the solution.

TEM images of MWCNTs, o-MWCNTs, GO and NH_2-SH-GO/MWCNTs are shown in Fig. 2. Fig. 2(a) shows that MWCNTs are cylindrical. The average diameter is 20–30 nm with lot of catalyst impurities on the surface and exist obvious aggregation. Fig. 2(b) shows that o-MWCNTs have no impurity. The surface is rough with lot of grooves and the ends are opened. Due to the oxidation, the average diameter of CNTs increases to 40–50 nm. Fig. 2(c) shows that GO has big lamellas and some drapes. Fig. 2(d) shows that NH_2-SH-GO/MWCNTs consists of graphene nanosheets and CNTs. Fig. 2(d) indicates that MWCNTs connect GO layers and some MWCNTs are closely attached to the surfaces of GO.

Fig. 3 shows SEM images of MWCNTs, o-MWCNTs, GO and NH_2-SH-GO/MWCNTs. Figs. 3(a) and (b) show that MWCNTs and o-MWCNTs are tubular, curved and tangled. Fig. 3(a) presents that MWCNTs are tortuous, randomly align with average diameter of 10–20 nm and length of 2 μm. Fig. 3(b) shows that after oxidation treatment, MWCNTs would be broken, length is shortened and there are some slight fragmentations to appear with length of 100 nm. Fig. 3(c) clearly reveals the folded, thin and layered structure of GO and the size is about 2 μm. Fig. 3(d) shows there are lot of MWCNTs and GO to interweave together. And there are some MWCNTs to adhere to the surface of GO [34]. Moreover,

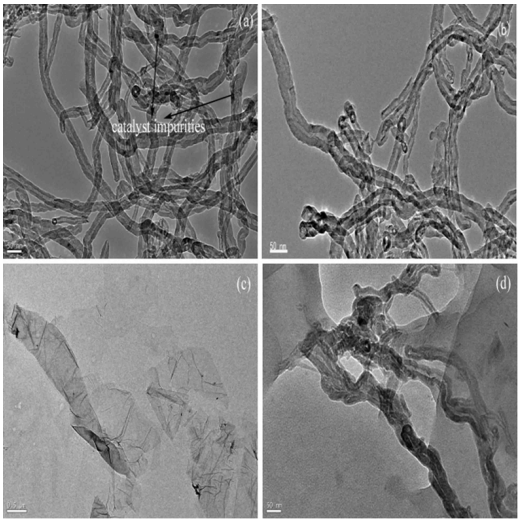

Fig. 2. TEM images of (a) MWCNTs, (b) o-MWCNTs, (c) GO and (d) NH_2-SH-GO/MWCNTs.

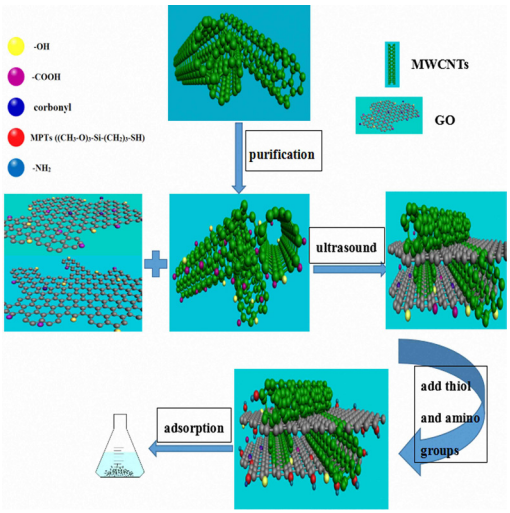

Fig. 1. Flow charts of NH_2-SH-GO/MWCNTs preparation and adsorption experiment.

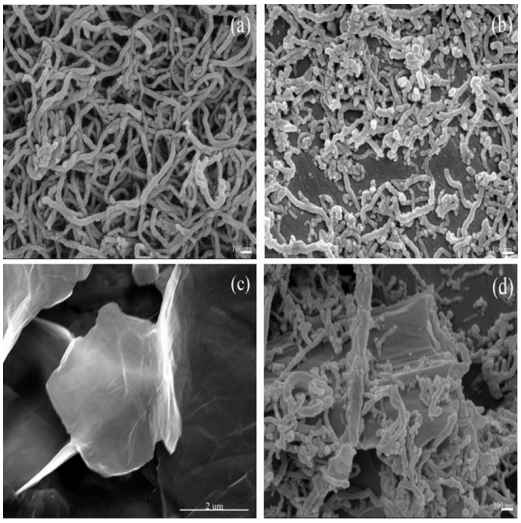

Fig. 3. SEM images of (a) MWCNTs, (b) o-MWCNTs, (c) GO and (d) NH_2-SH-GO/MWCNTs.

the rough surface of GO/MWCNTs is benefit for adsorption because it can provide more adsorption sites for pollutants.

3.2. FTIR spectra analysis

FTIR spectra were used to analyze functional groups of adsorbents. Fig. 4 shows FTIR spectra of NH_2-SH-GO/MWCNTs and GO/MWCNTs. The peak at 1,562 cm^{-1} is related to C=C stretching vibration (Fig. 4(a)). Fig. 4(b) shows some new peaks at 606 and 692 cm^{-1} are assigned to swing vibration of $–NH_2$ and wagging vibration of N–H, respectively [35,36]. The peak at 2,359 cm^{-1} is associated with $–NH_2$ stretching vibration [37]. The appearance of $–NH_2$ and N–H vibration peak indicates that amino groups appear on the surface of GO/MWCNTs. The results indicate that amino groups are present in the composites. Peaks at 721 and 805 cm^{-1} correspond to Si–C and Si–N stretching vibration, respectively. The results reveal that MPTS connect with MWCNTs or GO. And N_2H_4 and MPTS are also successfully connected. The peaks at 1,036 and 3,433 cm^{-1} are ascribed to stretching vibration of O–H and C–OH, respectively [38]. Peaks at 1,230 and 1,718 cm^{-1} are attributed to C–O and C=O stretching vibration in carboxylic acid, respectively. After oxidation of graphite and MWCNTs, a large number of oxygen-containing functional groups are introduced on the surface. Bands at 2,800–3,000 cm^{-1} are associated with symmetric and asymmetric stretching vibration of $–CH_2$. The enhanced intensity of $–CH_2$ stretching vibration indicates that additional methylene groups from MPTS are attached to the surface of GO/MWCNTs. Fig. 4(b) shows that a weak peak at 2,560 cm^{-1} may be assigned to S–H groups [39]. The peak at 1,106 cm^{-1} is attributed to Si–O stretching vibration. The appearance of Si–C and Si–O confirms that MPTS are grafted successfully on the surface of GO/MWCNTs. The new peak appearing at 1,445 cm^{-1} may be C–H stretching vibration [40]. These new peaks' appearance proves that MPTS and hydrazine are successfully coated on the GO/MWCNTs by connecting with these groups on the external surface of GO/MWCNTs.

3.3. Raman spectra analysis

Raman spectroscopy was used to detect structural modification of carbon materials after functionalization [41]. Fig. 5 shows Raman spectra of GO, GO/MWCNTs and NH_2-SH-GO/MWCNTs. Fig. 5(a) shows there are two strong peaks of GO. D peak at 1,301 cm^{-1} assigns to oxidizing defects. G band at 1,583 cm^{-1} relates to C–C stretching in the GO structure [42]. Fig. 5(b) shows Raman spectra of GO/MWCNTs and NH_2-SH-GO/MWCNTs. For GO/MWCNTs, D peak is at 1,365 cm^{-1} and G peak is presented at 1,660 cm^{-1}. The results indicate that peak positions shift to the lower frequency (blue shift). These changes should be the introduction of MWCNTs. For NH_2-SH-GO/MWCNTs, D peak at 1,355 cm^{-1} assigns to oxidizing defects or edge. Compared with that of GO/MWCNTs, G peak at 1,665 cm^{-1} that relates to C–C stretching vibration in the graphitic structure, are also shifted. There are new peaks in Fig. 5(b). The peak at 2,584 cm^{-1} may be –SH stretching vibration [43]. The peak at 1,024 cm^{-1} belongs to $–NH_2$ rocking vibration, which fits with FTIR spectra [44]. The bands at 714, 931, 1,118 and 2,937 cm^{-1} may be Si–O, Si–C, Si–N and $–CH_2$ stretching vibration, respectively. The intensity ratio between D and G peak is commonly used to evaluate the defective nature of sp^2 material, and relates with the degree of functionalization [45]. Fig. 5(a) shows that I_D/I_G ratio of GO is 1.113. I_D/I_G ratio of GO/MWCNTs is 1.098 and the ratio of NH_2-SH-GO/MWCNTs is 1.382 in Fig. 5(b), respectively. Comparing with GO/MWCNTs, I_D/I_G ratio of NH_2-SH-GO/MWCNTs increases. The results can evidence effective groups to associate with defects of composite.

3.4. TGA analysis

TGA is used to quantify quality of functional groups that presented on the surface of composite. Fig. 6 shows the TGA curves of GO/MWCNTs, SH-GO/MWCNTs and NH_2-SH-GO/MWCNTs. Fig. 6(a) presents the weight loss at the first stage is 3.8 wt% from 58.82°C to 102.13°C, which maybe the interlayer water to disappear. Weight loss at the second stage is about 17.81 wt% from 102.13°C to 225.14°C, where appears exothermic peak. The change can contribute to the thermal decomposition of vestigial hydrogen peroxide, nitrate ions and sulfate ions. Weight loss at the third stage is from 225.14°C to 1,098.36°C, which attribute to decomposition of groups, such as –COOH and –OH, on the surface of composite [46]. Fig. 6(b) shows that the weight loss of 8.09 wt% from 61.13°C to 356.24°C is consistent with the result in Fig. 6(a), and may also be the decomposition of acetic acid. The second weight loss is from 356.24°C to 631.72°C in Fig. 6(b) and the weight loss is up to 12.01 wt%. Based on the thermogravimetric result, it may be concluded that 12.01 wt% of sulfydryl is grafted onto the surface of GO/MWCNTs. Fig. 6(c) illustrates that the weight loss of 2.84 wt% is from 23.01°C to 178.36°C

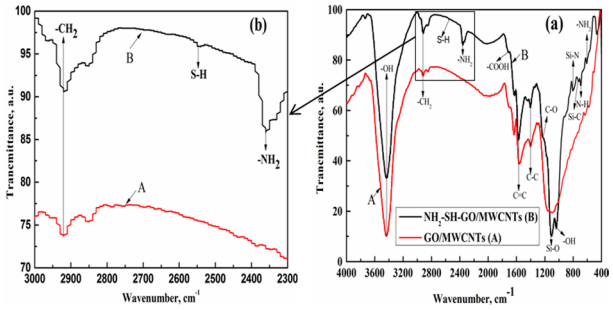

Fig. 4. FTIR spectra of (a) GO/MWCNTs and (b) NH_2-SH-GO/MWCNTs.

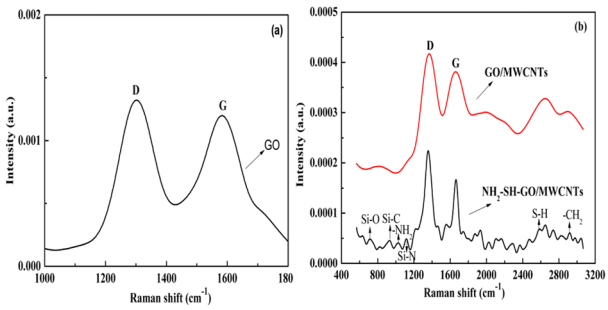

Fig. 5. Raman spectra of (a) GO and (b) GO/MWCNTs and NH_2-SH-GO/MWCNTs.

and there is also an obvious weight loss from 178.36°C to 356.24°C, where the weight loss is 6.1 wt%. The third weight loss is 21.91 wt% from 356.24°C to 623.63°C, which are the total weight of –SH and –NH_2 groups. And the content of amino groups is 10.75 wt%. All the results indicate that functional groups are successfully coated on the surfaces of composite, and NH_2-SH-GO/MWCNTs have a good thermal stability.

3.5. XRD pattern analysis

XRD pattern of graphite, GO, GO/MWCNTs and NH_2-SH-GO/MWCNTs are shown in Fig. 7. XRD pattern of graphite showed a very strong peak of (002) at 26.8° in Fig. 7(a) with interlayer distance of 0.332 nm. There was also a strong peak at 12.6°, which was according to (001) of GO

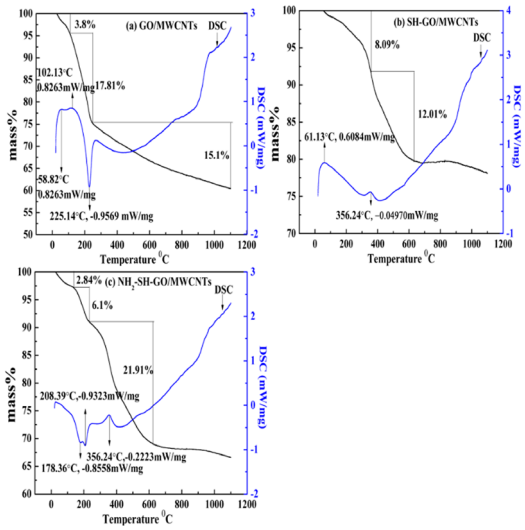

Fig. 6. TGA curves of (a) GO/MWCNTs, (b) SH-GO/MWCNTs and (c) NH_2-SH-GO/MWCNTs.

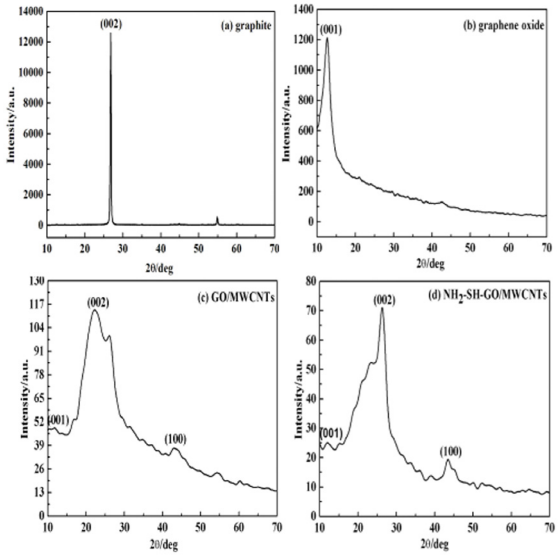

Fig. 7. XRD pattern of (a) graphite, (b) GO, (c) GO/MWCNTs and (d) NH_2-SH-GO/MWCNTs.

in Fig. 7(b) and the interlayer distance was 0.702 nm. The increase of interlayer distance was attributed to extensive oxidation of faces and edges [47]. Fig. 7(c) shows (001) of GO shifted to 11.8°, which corresponded to an interlayer distance of 0.749 nm. The increase of interlayer distance revealed MWCNTs successfully interweaved with GO together. And there were new peaks to appear in Fig. 7(c), which corresponded to (002) and (100) of MWCNTs to appear. The result may be caused by introducing CNTs [48]. There was also a peak at 12.56° to appear, which attributed to (001) of GO. But it can be seen that the peak was very weak, and characteristic peak of GO was very sharp in Fig. 7(b). Besides characteristic peak of MWCNTs that was at 26.4° and 42.8°, corresponded to (002) and (100), respectively. Compared with the peaks of MWCNTs, the peak intensity of GO/MWCNTs was weak. XRD pattern of GO/MWCNTs is not a simple super position that diffraction peak of MWCNTs and GO. The material is not mixture. Fig. 7(d) shows a shift of (001) to 11.9°, which corresponds to an interlayer distance of 0.743 nm. And (002) and (100) also changed to 26.3° and 43.4°, respectively. Compared with that of GO/MWCNTs, a decrease of interlayer distance may be caused by reduction of GO as some amino groups are introduced [49].

3.6. XPS analysis

XPS is typically considered to be helpful for identifying groups and surface elements of composites. Table 2 shows the energy, peak area and atomic percentage of NH_2-SH-GO/MWCNTs. The data reveal the presence of carbon, oxygen, nitrogen, sulfur and silicon elements in NH_2-SH-GO/MWCNTs. The atomic percentage of C, O, N, S and Si can reach 80.58%, 12.61%, 2.39%, 1.99% and 2.43%, respectively. These data indicated that the functional groups, such as amino and sulfydryl groups, were successfully grafted on the surface of GO/MWCNTs. The experimental data were fitted with Gaussian components soft and the best fits are plotted in the figure. C1s, O1s, N1s, S2p and Si2p peaks of NH_2-SH-GO/MWCNTs are clearly observed in Fig. 8(a). The strong C1s peak at 284.39 eV corresponds to MWCNTs and GO. The binding energy at 530.66 eV is attributed to O1s. Peaks at 164.51 and 101.32 eV are corresponding to S2p and Si2p, respectively, which appear in MPTS. N1s peak is from hydrazine at 400.25 eV. Fig. 8(b) shows that C1s spectrum of NH_2-SH-GO/MWCNTs can be deconvoluted into three Gaussian peaks which centered at 284.77, 285.13 and 285.06 eV [50] (corresponding to C=C, C=O and C–OH, respectively). Fig. 8(c) indicates the Gaussian peaks are assigned to C–O, C–OH and C=O–OH (530.62, 532.56 and 533.08 eV [51], respectively).

Table 2
The energy, peak area and atomic percentage of NH_2-SH-GO/MWCNTs

Name	Energy (eV)	Peak area (%)	Atomic percentage (%)
C1s	284.39	64.84	80.58
O1s	530.66	26.96	12.61
N1s	400.25	3.40	2.39
S2p	164.51	2.64	1.99
Si2p	101.32	2.16	2.43

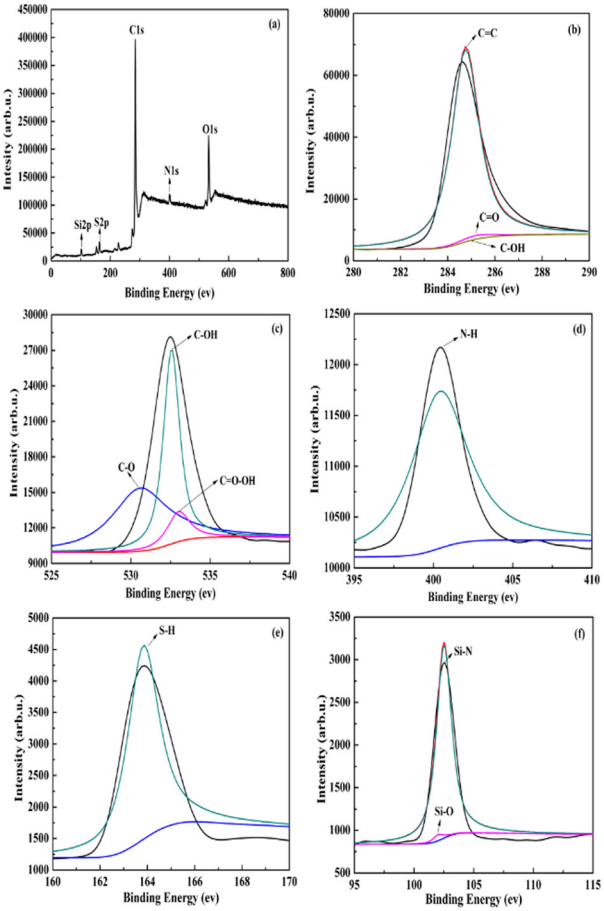

Fig. 8. XPS wide scan of (a) NH_2-SH-GO/MWCNTs, (b) C1s, (c) O1s, (d) N1s, (e) S2p and (f) Si2p.

The results of O1s spectra are consistent with C1s spectra. Figs. 8(d) and (e) show that Gaussian peaks assigning to N–H and S–H are detected at 400.42 and 163.85 eV, respectively [52]. In addition, Gaussian peaks of Si–N and Si–O appear at 102.53 and 101.98 eV in Fig. 8(f). The appearance of Si–O peak can prove that MPTS is coated on the surface of composite, and the results are consistent with the FTIR spectra result. According to the results of XPS and FTIR, NH_2-SH-GO/MWCNTs were successfully prepared using the experimental method.

3.7. Nitrogen adsorption–desorption isotherm

Textural parameters such as Brunauer–Emmett–Teller (BET) surface area, Barrett–Joyner–Halenda pore size distribution of NH_2-SH-GO/MWCNTs, were obtained from nitrogen adsorption–desorption isotherms and are shown in Fig. 9. The isotherms of NH_2-SH-GO/MWCNTs display a slow rise under low relative pressure, indicating these composites are mesoporous or macropore materials. A second rise at high relative pressure reveals the existence of macropore. This type belongs to type V with hysteresis loops at relative pressure (P/P_0) between 0.4 and 1.0, which confirms the mesoporous feature. Type V indicates the existence of weaker interaction forces between adsorbate and adsorbent. In addition, according to the pore size distribution curve, the major

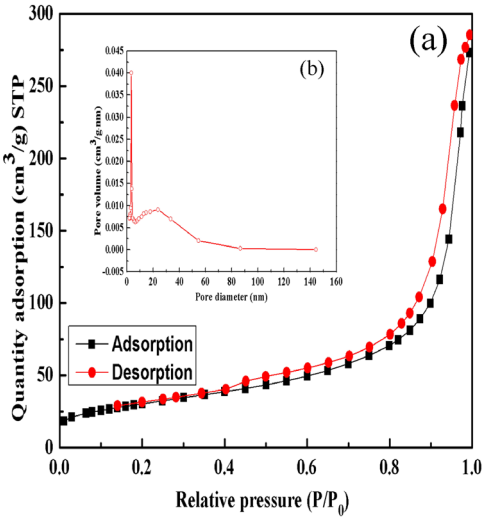

Fig. 9. Nitrogen adsorption–desorption isotherm and pore size distribution curve (the inset pattern) of NH_2-SH-GO/MWCNTs.

pore diameter is less than 20 nm but more than 2 nm. The average pore diameter is about 12.29 nm, which suggests that NH_2-SH-GO/MWCNTs belong to mesoporous material. The BET analysis indicates that specific surface areas of NH_2-SH-GO/MWCNTs are 109.68 m^2/g. But the obtained value is much lower, which may be the incomplete exfoliation and the nonporous GO as well as the coacervate of CNTs [53].

3.8. Effects of pH on adsorption

The pH values affecting on the adsorbate adsorption on NH_2-SH-GO/MWCNTs can be attributed to ion exchange, surface complexation and electrostatic interactions with its oxygen-containing groups [54]. In the present study, pH values varied between 2 and 9 to avoid forming hydroxide precipitation of lead and zinc ions. At high pH over 9, lead hydroxide became predominant and subsequently the precipitation of zinc hydroxide occurred. And at pH lower than 9, the predominant zinc species was always Zn^{2+}. Thus, the adsorption experiments were conducted by varying the solution pH over the range of 2.0–9.0 to avoid the contribution from lead and zinc hydroxide precipitation. Other experimental factors were kept for 8 h at room temperature. The adsorbent dosage was 25 mg/L and the adsorbate concentration was 10 mg/L.

Fig. 10 shows that the maximum adsorption capacity at equilibrium is 125.8, 98.6 and 23.8 mg/g for Pb^{2+}, Zn^{2+} and phenol, respectively. Fig. 10 illustrates that the equilibrium adsorption capacity of NH_2-SH-GO/MWCNTs for Pb^{2+} and Zn^{2+} increases rapidly as pH increases from 2.0 to 5.0. There is electrostatic attraction between the negative charged sites of adsorbents and the positive charges of metal ions. Moreover, although the adsorption capacity at equilibrium for phenol also increases as pH value changes from 2.0 to 5.0. Sun et al. [55] demonstrated that GO and MWCNTs presented the negative charges at pH > 2.0. Therefore, the increasing adsorption capacity of NH_2-SH-GO/MWCNTs could be attributed to the strong electrostatic attraction between adsorbent with negative charges and metal ions with positive charges.

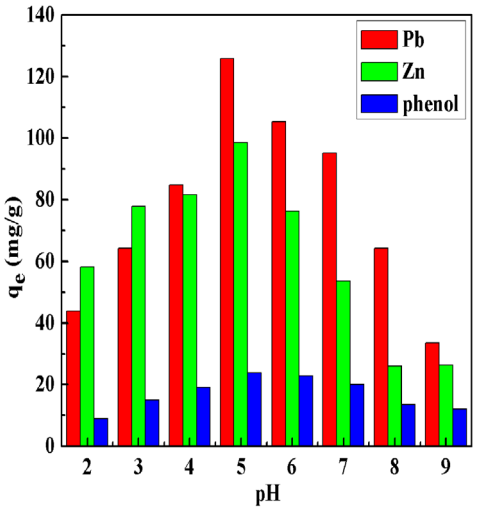

Fig. 10. Effects of pH on adsorption capacity of NH_2-SH-GO/MWCNTs for Pb^{2+}, Zn^{2+} and phenol.

The adsorption capacity at equilibrium is low as pH value is below 5.0, which attributes to the competition of H^+ that can compete with Pb^{2+}, Zn^{2+} and phenol for the adsorption sites. These hydrogen ions prevent the target ions from adsorbing on the surface of the composite. This conclusion was the same with the surface complex formation theory, which proved that as the hydrogen ions increased, competition for the adsorption sites between proton and metal species was increased [56]. More metal ions are adsorbed with the decrease of positive charges. As pH increased to be more than 5.0, the adsorption capacity at equilibrium decreased because of the combined roles of adsorption and precipitation of Pb^{2+} and Zn^{2+} as $Pb(OH)_2$ and $Zn(OH)_2$, respectively. The hydrolysis pH of Zn^{2+} and Pb^{2+} was 6.54 and 7.04, respectively. At the beginning of adsorption, the surface is empty and more phenol adsorbed on the surface of NH_2-SH-GO/MWCNTs by electrostatic attraction and van der Waals force. With the further increase of pH value, increasing hydroxyl ions make phenol with negative charges. And the surface of adsorbent with negative charges, make the adsorption capacity for phenol decrease [57].

3.9. Effects of contact time and adsorption kinetics

The effects of contact time on Pb^{2+}, Zn^{2+} and phenol adsorption on the NH_2-SH-GO/MWCNTs were studied at room temperature. Fig. 11 shows that the adsorption capacity of NH_2-SH-GO/MWCNTs for Pb^{2+}, Zn^{2+} and phenol adsorption increased gradually until equilibrium was reached after 60 min, which could be due to the rapid diffusion of adsorbates towards NH_2-SH-GO/MWCNTs. The adsorption capacity of NH_2-SH-GO/MWCNTs at 60 min was 125.8, 98.6 and 23.8 mg/g for Pb^{2+}, Zn^{2+} and phenol, respectively. Then, adsorption capacity kept stable from 60 min to 36 h. The subsequent slow adsorption capacity was attributed to long diffusion of adsorbates into the inner layers sites of GO [58]. Therefore, the long contact time (8 h) was selected in the following adsorption experiments

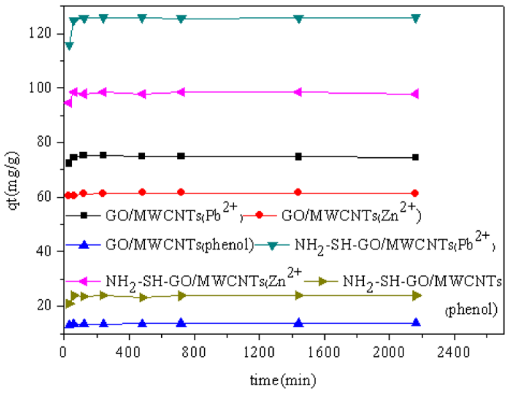

Fig. 11. Effects of contact time on Pb^{2+}, Zn^{2+} and phenol adsorption (initial condition: 2.5 mg NH_2-SH-GO/MWCNTs, 10 mg/L Pb^{2+}, Zn^{2+} and phenol at pH 5).

in order to reach complete adsorption equilibrium. To compare adsorption capacity between NH_2-SH-GO/MWCNTs and GO/MWCNTs, the curves are shown in Fig. 11. Fig. 11 indicates the adsorption capacity of NH_2-SH-GO/MWCNTs for Pb^{2+}, Zn^{2+} and phenol adsorption is better than that of GO/MWCNTs. The adsorption capacity of NH_2-SH-GO/MWCNTs for Pb^{2+} adsorption was 125.8 mg/g, however, adsorption capacity of GO/MWCNTs was 75 mg/g. The phenomenon is similar for Zn^{2+} and phenol adsorption. The results indicated that the performance of our prepared adsorbent is superior to nonfunctionalization material. The adsorption kinetics data of Pb^{2+}, Zn^{2+} and phenol onto NH_2-SH-GO/MWCNTs were analyzed with two different kinetics models: pseudo-first-order model and pseudo-second-order model, respectively. The kinetics studies were carried out by investigating the possible adsorption mechanism, equilibrium time, adsorption rates and interaction between adsorbent and pollutants. The linear plots of kinetics model for different concentrations of lead ions (or zinc and phenol) are shown in Figs. 12 and 13. The obtained values of k_1, calculated q_e values and coefficients of R^2 for Pb^{2+} (or Zn^{2+} and phenol) in NH_2-SH-GO/MWCNTs were given in Table 3.

Figs. 12 and 13 show pseudo-first-order and pseudo-second-order kinetics models for Pb^{2+}, Zn^{2+} and phenol adsorption. Table 3 indicates the parameters of pseudo-first-order and pseudo-second-order equation which calculates from the slope and intercept. Table 3 clearly indicates that the experimental data fit well with pseudo-second-order kinetics model with higher R^2. And there are strong chemical forces between adsorbent and adsorbates, which is caused by strong surface complexation of metal ions with the functional groups on the surface of GO/MWCNTs, especially amino and sulfydryl groups. The R^2 values of pseudo-second-order model are higher than that of pseudo-first-order model. In addition, the calculated values of adsorption capacity at equilibrium (q_{ca}) from the pseudo-second-order kinetics are 125.6, 98.4 and 23.8 mg/g for Pb^{2+}, Zn^{2+} and phenol, respectively. The data are better fitted to the experimental data (125.8, 98.6 and 23.8 mg/g, respectively) than that of pseudo-first-order model. The initial adsorption rate (h) which calculated from

pseudo-second-order rate equation for Pb^{2+}, Zn^{2+} and phenol are 549.45, 135.55 and 38.01 mg/g min, respectively. The result indicates that adsorption rate for Pb^{2+} is faster than that of Zn^{2+} and phenol.

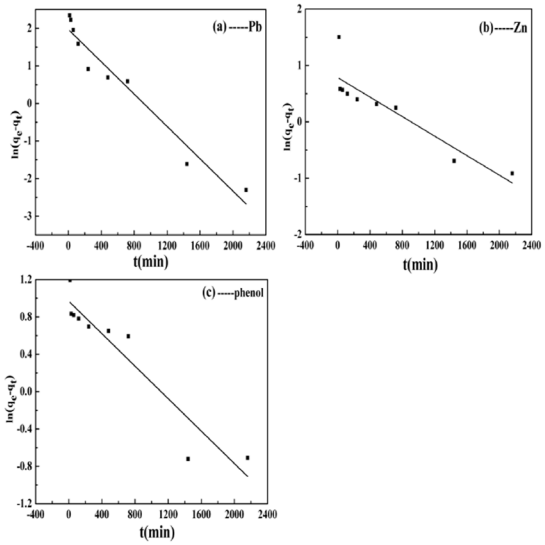

Fig. 12. Pseudo-first-order kinetic model for (a) Pb^{2+}, (b) Zn^{2+} and (c) phenol adsorption.

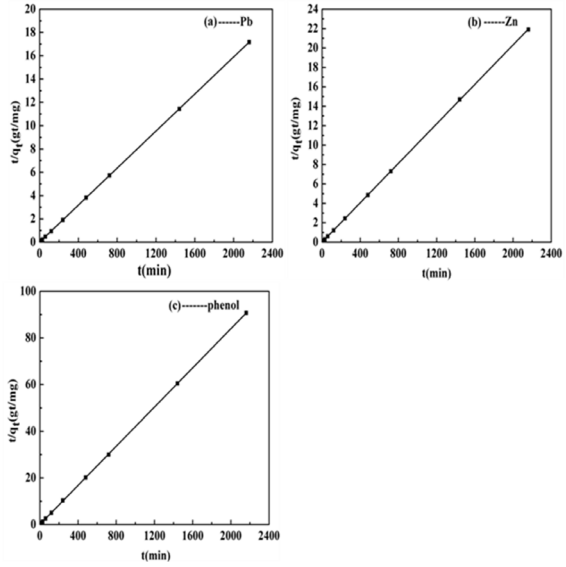

Fig. 13. Pseudo-second-order kinetic model for (a) Pb^{2+}, (b) Zn^{2+} and (c) phenol adsorption.

3.10. Isotherm models

Analysis of isotherm data by fitting them to different models is an important step to investigate how adsorption molecules distribute between the liquid phase and the solid phase as the adsorption process reaches an equilibrium state [59]. The original adsorption data of Langmuir and Freundlich isotherm models for Pb^{2+}, Zn^{2+} and phenol adsorption are shown in Table 4. In the present study, Langmuir and Freundlich isotherm models are used to fit the original adsorption data of Pb^{2+}, Zn^{2+} and phenol. Langmuir and Freundlich isotherm models are presented in Figs. 11 and 12 and their parameters are summarized in Table 5.

Figs. 14 and 15 show isotherm models for Pb^{2+}, Zn^{2+} and phenol adsorption on the surface of NH_2-SH-GO/MWCNTs. Table 4 shows that Pb^{2+}, Zn^{2+} and phenol adsorption fits Freundlich isotherm model with higher R^2 values. The data reveal that Pb^{2+}, Zn^{2+} and phenol adsorption may be occurred as a multilayer adsorption [60]. NH_2-SH-GO/MWCNTs can provide and form specific binding capability by strong bidentate ligand in the solution due to their groups which grafted on the GO/MWCNTs surface. The binding capability results in the formation of binding sites [61]. So these structures can provide varieties of adsorption sites for Pb^{2+}, Zn^{2+} and phenol. The R^2 of Freundlich isotherm model for Pb^{2+}, Zn^{2+} and phenol is 0.98, 0.97 and 0.97, respectively, which are higher than that of Langmuir isotherm model. Therefore, Freundlich isotherm model can fit data better than Langmuir isotherm model. The n values of Pb^{2+} and Zn^{2+} adsorption are more than 1 and phenol is less than 1, which indicates that a favorable condition for Pb^{2+} and Zn^{2+} adsorption but for phenol is disadvantageous. The results also explain the reason that the adsorption capacity of NH_2-SH-GO/MWCNTs for phenol is lower than that of Pb^{2+} and Zn^{2+}.

Table 4
The original adsorption data of Langmuir and Freundlich isotherm models for Pb^{2+}, Zn^{2+} and phenol adsorption

Pb^{2+}		Zn^{2+}		Phenol	
C_e (mg/L)	q_e (mg/g)	C_e (mg/L)	q_e (mg/g)	C_e (mg/L)	q_e (mg/g)
3.01	79.7	3.26	69.6	4.52	19.1
7.11	115.6	7.54	98.6	9.41	23.8
10.9	161.7	11.24	150.4	13.71	51.5
14.0	238.7	14.84	206.3	17.6	96.2
17.37	305.3	18.42	263.2	22.29	108.3

Table 3
The parameters of pseudo-first-order and pseudo-second-order models for Pb^{2+}, Zn^{2+} and phenol adsorption

Adsorbate	Pseudo-first-order				Pseudo-second-order			
	q_{ex} (mg/g)	q_{ca} (mg/g)	k_1R^2 (1/min)		q_{ex} (mg/g)	q_{ca} (mg/g)	k_2R^2 (g/mg/min)	
Pb^{2+}	125.8	7.17	0.00215	0.94	125.8	125.78	0.035	0.999
Zn^{2+}	98.6	2.19	0.00087	0.79	98.6	98.14	0.014	0.999
Phenol	23.8	2.63	0.00087	0.88	23.8	23.82	0.067	0.999

Table 5
The parameters of Langmuir and Freundlich isotherm models for Pb^{2+}, Zn^{2+} and phenol adsorption on the NH_2-SH-GO/MWCNTs

Adsorbate	Langmuir isotherm model			Freundlich isotherm model		
	q_m (mg/g)	b (L/mg)	R^2	K_f (mmol^{1-n}·L^n/kg)	n	R^2
Pb^{2+}	1.065	0.00034	0.87	4.582	1.336	0.98
Zn^{2+}	1.074	0.00023	0.93	4.212	1.34	0.97
Phenol	1.277	0.00191	0.83	1.737	0.938	0.97

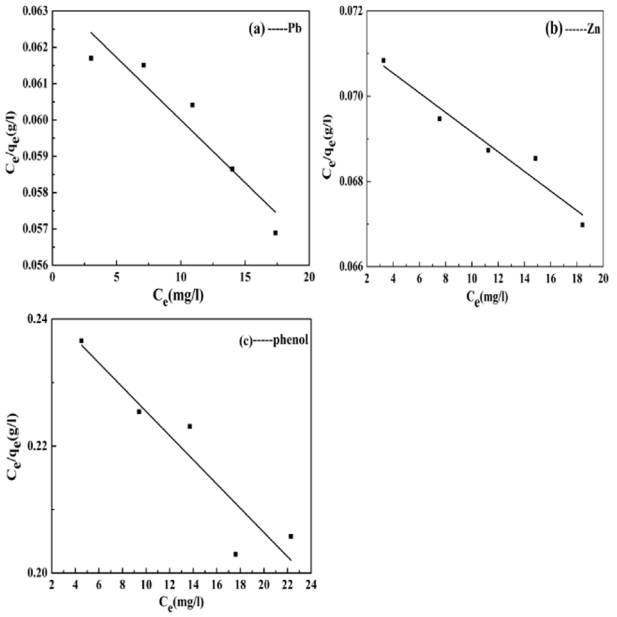

Fig. 14. Langmuir isotherm model for (a) Pb^{2+}, (b) Zn^{2+} and (c) phenol adsorption on the NH_2-SH-GO/MWCNTs.

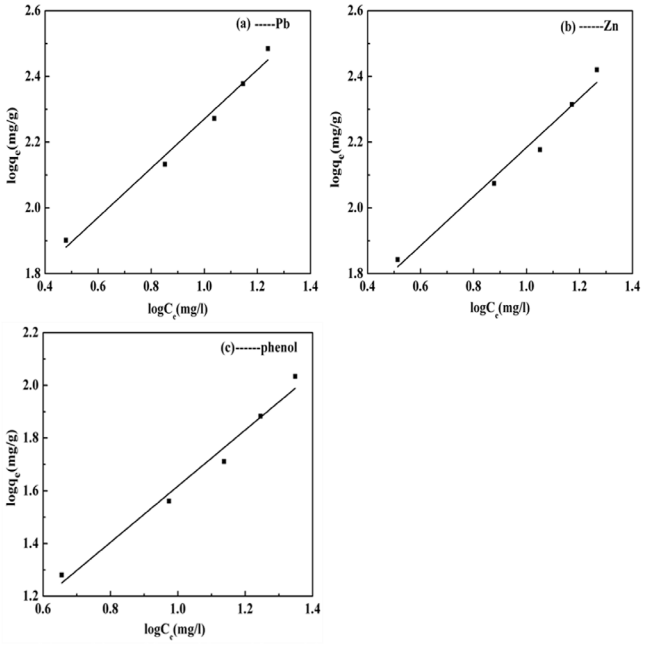

Fig. 15. Freundlich isotherm model for (a) Pb^{2+}, (b) Zn^{2+} and (c) phenol adsorption on the NH_2-SH-GO/MWCNTs.

3.11. Adsorption thermodynamics

Thermodynamics parameters explained the interactions between adsorbent and solute, as well as the resulting energy changes in the adsorption process. The Gibbs free energy, enthalpy and entropy were determined by the following equations [62]:

$$K_d = \frac{(C_0 - C_e)V}{mC_e} \tag{7}$$

$$\ln K_d = \frac{\Delta S^\theta}{R} - \frac{\Delta H^\theta}{RT} \tag{8}$$

$$\Delta G^\theta = \Delta H^\theta - T\Delta S^\theta \tag{9}$$

where K_d represents the distribution ratio (L/g); C_0 and C_e represent initial concentration and concentration at equilibrium (mg/L), respectively; V is the volume of adsorbate solution (L) and m is the weight of adsorbent (g); ΔG^θ, ΔH^θ and ΔS^θ are the change of standard free energy (kJ/mol), enthalpy (J/mol) and entropy (J/mol·K^{-1}), respectively; R is the universal gas constant of 8.314 J/mol·K and T is the absolute temperature (K).

Fig. 16 shows that the relationship between lnK_d and 1/T. Table 6 shows that the distribution ratio of K_d increase with rising temperatures, indicating the endothermic nature of adsorption. The values of ΔH^θ and ΔS^θ are obtained from the slope and intercept of the plots. The thermodynamic parameters of Gibbs free energy change (ΔG^θ) are shown in Table 6. Generally speaking, change of ΔG^θ for physisorption occurs between –20 and 0 kJ/mol, while chemisorption occurs in the range of –80 to –400 kJ/mol [63]. The negative values of ΔG^θ at various temperatures indicate the adsorption of adsorbates on NH-SH-GO/MWCNTs is favorably spontaneous process and attributed to physisorption. The positive values of ΔS^θ indicate that adsorption process is random in the solid and solution interface. The positive values of ΔH^θ indicate that the adsorption process is endothermic [64].

3.12. The recycle times of NH_2-SH-GO/MWCNTs

In order to research the regeneration and recycle times of composite, adsorption experiments are performed. The steps of recycle experiment are as follows: first, take 100 mL Pb^{2+}, Zn^{2+} ions and phenol solution (10 mg/L), adjusts pH value of the solution to be 5, then the concentration of NH_2-SH-GO/MWCNTs is set to 25 mg/L at 25°C for 12 h.

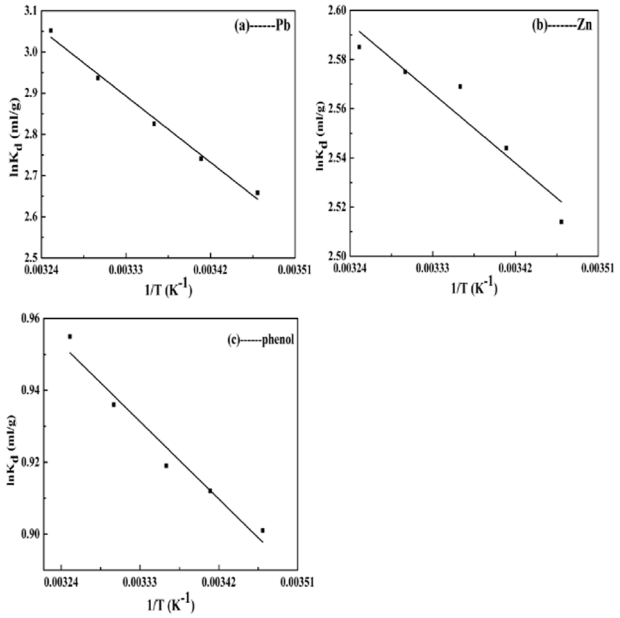

Fig. 16. Plots of lnK_d and 1/T relationship for (a) Pb^{2+}, (b) Zn^{2+} and (c) phenol adsorption.

Table 6
Thermodynamic parameters for Pb^{2+}, Zn^{2+} and phenol adsorption on the surface of NH_2-SH-GO/MWCNTs at different temperatures

T (K)		lnK_d	ΔG^θ (kJ/mol)	ΔH^θ (kJ/mol)	ΔS^θ (J/mol K)
Pb^{2+}	288	2.658	–6.319	14.849	73.499
	293	2.741	–6.686		
	298	2.826	–7.054		
	303	2.937	–7.421		
	308	3.052	–7.789		
Zn^{2+}	288	2.514	–6.038	2.618	30.055
	293	2.544	–6.188		
	298	2.569	–6.338		
	303	2.575	–6.489		
	308	2.585	–6.639		
Phenol	288	0.901	–2.148	1.992	14.375
	293	0.912	–2.220		
	298	0.919	–2.292		
	303	0.937	–2.364		
	308	0.955	–2.436		

After adsorption experiment, the concentration of Pb^{2+}, Zn^{2+} and phenol is measured. After immersing NH_2-SH-GO/MWCNTs with 1% HCl solution for 2 h, and then washed several times with deionized water. The same adsorption experiment is carried out again. Then, the wash-adsorption experiment is carried out for six cycles. After each cycle, the adsorption capacities of adsorbent are calculated. Fig. 17 shows the recycle times of NH_2-SH-GO/MWCNTs for Pb^{2+}, Zn^{2+} and phenol. It can be obtained that with the increase of recycle times, adsorption capacities of NH_2-SH-GO/MWCNTs reduce for Pb^{2+}, Zn^{2+} and phenol. The adsorption capacities of adsorbent for Pb^{2+}, Zn^{2+} ions and phenol are 127.2, 97.2 and 23.4 mg/g at the first time, respectively. Comparing with adsorption capacity at the first time, adsorption capacity reduces by 5.19% for Pb^{2+} at the second time. The phenomenon is similar for Zn^{2+} ions and phenol adsorption. The adsorption capacities of adsorbent for Pb^{2+}, Zn^{2+} and phenol reduce by 36.55%, 30.86% and 25.64% after six times. Although adsorption capacities of adsorbent reduce, NH_2-SH-GO/MWCNTs remain high adsorption capacity. The above results show that NH_2-SH-GO/MWCNTs can be used for several times to reduce the costs of wastewater treatment.

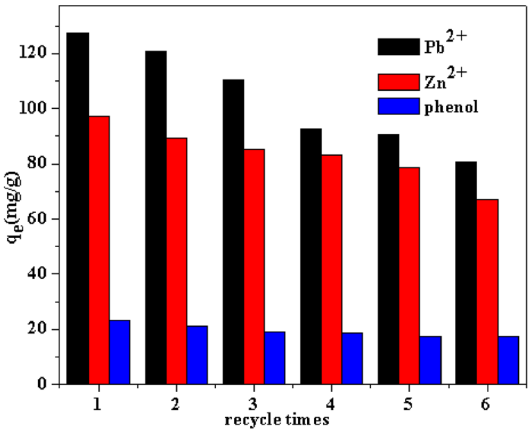

Fig. 17. The recycle times of NH_2-SH-GO/MWCNTs for Pb^{2+}, Zn^{2+} and phenol adsorption.

4. Conclusion

We have successfully prepared NH_2-SH-GO/MWCNTs with a simple and high-yield way. TEM and SEM images proved that some MWCNTs closely attached to the surface of the GO nanosheets and some inserted into GO nanosheets. The results of FTIR revealed that GO/MWCNTs were functionalized by sulfydryl and amino groups. The nitrogen adsorption–desorption isotherm showed that composite was mesoporous. The present investigation showed that NH_2-SH-GO/MWCNTs was an effective adsorbent for the removal of Pb^{2+}, Zn^{2+} and phenol from aqueous solution. The optimum conditions for the adsorption process were found to be 480 min for contact time, at pH 5 and adsorbent doses of 25 mg/L. Pseudo-second-order kinetic model can well describe the adsorption process. The equilibrium adsorption data fit better with Freundlich isotherm model than Langmuir model. Based on Freundlich isotherm model, the maximum adsorption capacity of NH_2-SH-GO/MWCNTs was 125.8, 98.6 and 23.8 mg/g for Pb^{2+}, Zn^{2+} and phenol, respectively. Thermodynamic results showed that adsorption process was spontaneous and endothermic. ΔG^θ values indicated that interactions belong to physisorption. In a word, it can be concluded that NH_2-SH-GO/MWCNTs offer a new, potential and highly efficient adsorbent which can be applied for wastewater treatment systems.

Acknowledgments

This study was funded by National Nature Science Foundation of China (51304101 and 51764039), Scientific and Research Project of Institutions of Higher Learning in Gansu Province (2015B-033), and Youth Science and Technology Fund Project of Gansu Province (1606RJYA305).

Conflict of interest

The authors declare that they have no conflict of interest.

Symbols

b	—	Energy of adsorption, L/mg
C_0	—	Initial concentration of adsorbate in solution, mg/L
C_e	—	Concentration of adsorbate at equilibrium, mg/L
h	—	Initial rate of adsorption, as time is nearly to zero, mg/g·min
k_1	—	Pseudo-first-order rate constant, 1/min
k_2	—	Pseudo-second-order rate constant, g/mg/min
K_d	—	Distribution ratio, L/g
K_f	—	Freundlich constants related to the adsorption capacity, $mmol^{1-n}\cdot L^n/kg$
m	—	Weight of adsorbent, g
n	—	Freundlich constants related to adsorption intensity, dimensionless
q_e	—	Adsorption capacity of adsorbent at equilibrium, mg/g
q_{max}	—	Maximum adsorption capacity, mg/g
q_t	—	Adsorption capacity of adsorbent at equilibrium at time of t, mg/g
R	—	Universal gas constant of 8.314 J/mol·K
T	—	Absolute temperature, K
t	—	Time, min
V	—	Volume of solution, L
ΔG^θ	—	Standard Gibb free energy change, kJ/mol
ΔH^θ	—	Standard enthalpy, J/mol
ΔS^θ	—	Standard entropy, $J/mol\cdot K^{-1}$

References

[1] A. Corami, S. Mignardi, V. Ferrini, Cadmium removal from single- and multi-metal solutions by sorption on hydroxyapatite, J. Colloid Interface Sci., 317 (2008) 402–408.
[2] N.T. Abdel-Ghani, G.A. El-Chaghaby, F.S. Helal, Individual and competitive adsorption of phenol and nickel onto multiwalled carbon nanotubes, J. Adv. Res., 6 (2014) 405–415.
[3] N. Guo, Y.M. Liang, S. Lan, L. Liu, G.J. Ji, S.C. Gan, H.F. Zou, X.C. Xu, Uniform TiO-SiO hollow nanospheres: synthesis, characterization and enhanced adsorption photodegradation of azo dyes and phenol, Appl. Surf. Sci., 305 (2014) 562–574.
[4] P. Muchez, M. Corbella, Factors controlling the precipitation of copper and cobalt minerals in sediment-hosted ore deposits: advances and restrictions, J. Geochem. Explor., 118 (2006) 38–46.
[5] S. Oh, T. Kang, H. Kim, J. Moon, S. Hong, J. Yi, Preparation of novel ceramic membranes modified by mesoporous silica with 3-aminopropyltriethoxysilane (APTES) and its application to Cu^{2+} separation in the aqueous phase, J. Membr. Sci., 301 (2007) 118–125.
[6] J.J. Chuechill, M.W. Beutel, P.S. Burgoon, Evaluation of optimal dose and mixing regime for alum treatment of Matthiesen Creek inflow to Jameson Lake, Washington, Lake Reservoir Manage., 25 (2009) 102–110.
[7] P.K. Jal, S. Patel, B.K. Mishra, Chemical modification of silica surface by immobilization of functional groups for extractive concentration of metal ions, Talanta, 62 (2004) 1005–1028.
[8] X. Liu, J.X. Li, X.X. Wang, C.L. Chen, X.K. Wang, High performance of phosphate-functionalized graphene oxide for the selective adsorption of U(VI) from acidic solution, J. Nucl. Mater., 466 (2015) 56–64.
[9] Z. Wei, Y. Seo, Trichloroethylene (TCE) adsorption using sustainable organic mulch, J. Hazard. Mater., 181 (2010) 147–153.
[10] A.K. Geim, K.S. Novoselov, The rise of graphene, Nat. Mater., 6 (2007) 183–191.
[11] S. Lijima, Helical microtubules of graphic carbon, Nature, 354 (1991) 56–58.
[12] Y. Zhu, S. Murali, W. Cai, X. Li, J.W. Suk, J.R. Potts, R.S. Ruoff, Graphene and graphene oxide: synthesis, properties, and application, Adv. Mater., 22 (2010) 3906–3924.
[13] C.B. Wade, C. Thurman, W. Freas, J. Student, D. Matty, D.K. Mohanty, Preparation and characterization of high efficiency modified activated carbon for the capture of mercury from flue gas in coal-fired power plants, Fuel Process. Technol., 97 (2012) 107–117.
[14] M.D. Stoller, S. Park, Y. Zhu, J. An, R.S. Rouff, Graphene-based ultracapacitors, Nano Lett., 8 (2008) 3498–3502.
[15] J. Gong, J. Liu, Z.W. Jiang, X. Wen, E. Mijowska, T. Tang, X.C. Chen, A facile approach to prepare porous cup-stacked carbon nanotube with high performance in adsorption of methylene blue, J. Colloid Interface Sci., 445 (2015) 195–204.
[16] S. Wang, Y. Peng, Natural zeolites as effective adsorbents in water and wastewater treatment, Chem. Eng. J., 156 (2010) 11–24.
[17] P. Liang, Y. Liu, L. Guo, J. Zeng, H. Lu, Multiwalled carbon nanotubes as solid-phase extraction adsorbent for the preconcentration of trace metal ions and their determination by inductively coupled plasma atomic emission spectrometry, J. Anal. At. Spectrom., 19 (2004) 1489–1492.
[18] Y.S. Ho, G. Mckay, The kinetics of sorption of basic dyes from aqueous solution by sphagnum moss peat, Can. J. Chem. Eng., 76 (1998) 822–827.
[19] C.V. Pham, M. Eck, M. Krueger, Sulfydryl functionalized reduced graphene oxide as a base material for novel graphene-nanoparticle hybrid composites, J. Chem. Eng., 231 (2013) 146–154.
[20] A.H. El-Sheikh, Y.S. Al-Degs, R.M. Al-As'ad, J.A. Sweileh, Effect of oxidation and geometrical dimensions of carbon nanotubes on Hg(II) sorption and preconcentration from real waters, Desalination, 270 (2011) 214–220.
[21] J. Liu, H.Y. Du, S.W. Yuan, W.X. He, Z.H. Liu, Synthesis of sulfydryl-functionalized magnetic graphene as adsorbent for Cd(II) removal from aqueous systems, J. Environ. Chem. Eng., 3 (2015) 617–621.
[22] X.Y. Zhang, Q. Huang, M.Y. Liu, J.W. Tian, G.J. Zeng, Z. Li, K. Wang, Q.S. Zhang, Q. Wan, F.J. Deng, Y. Wei, Preparation of amine functionalized carbon nanotubes via a bioinspired strategy and their application in Cu^{2+} removal, Appl. Surf. Sci., 343 (2015) 19–27.
[23] L.L. Jiang, S.J. Li, H.T. Yu, Z.S. Zou, X.G. Hou, F.M. Shen, C.T. Li, X.Y. Yao, Amino and thiol modified magnetic multi-walled carbon nanotubes for the simultaneous removal of lead, zinc and phenol from aqueous solutions, Appl. Surf. Sci., 369 (2016) 398–413.
[24] C. Zhang, J. Sui, Y. Tang, W. Cai, Efficient removal of heavy metal ions by sulfydryl-functionalized super paramagnetic carbon nanotubes, Chem. Eng. J., 210 (2012) 45–52.
[25] W. Zhang, X. Shi, Y. Zhang, W. Gu, B. Li, Y. Xian, Synthesis of water-soluble magnetic graphene nanocomposites for recyclable removal of heavy metal ions, Mater. Chem. A, 5 (2013) 1745–1753.
[26] P.F. Wang, M.H. Cao, C. Wang, Y.H. Ao, J. Hou, J. Qian, Kinetics and thermodynamics of adsorption of methylene blue by a magnetic graphene-carbon nanotube composite, Appl. Surf. Sci., 290 (2014) 116–124.

[27] S.F. Hou, S.J. Su, M.L. Kasner, P. Shah, K. Patel, C.J. Madarang, Formation of highly stable dispersions of silane-functionalized reduced graphene oxide, Chem. Phys. Lett., 501 (2010) 68–74.
[28] N.T. Abdel-Ghani, G.A. El-Chaghaby, F.S. Helal, Individual and competitive adsorption of phenol and nickel onto multiwalled carbon nanotubes, J. Adv. Res., 6 (2014) 1–11.
[29] C.C. Huang, J.C. He, Electrosorptive removal of copper ions from wastewater by using ordered mesoporous carbon electrodes, Chem. Eng. J., 221 (2013) 469–475.
[30] T. Sheela, Y. Arthoba Nayaka, R. Viswanatha, S. Basavanna, T.G. Venkatesha, Kinetics and thermodynamics studies on the adsorption of Zn(II), Cd(II) and Hg(II) from aqueous solution using zinc oxide nanoparticles, Powder Technol., 217 (2012) 163–170.
[31] I. Langmuir, Adsorption of gases on plane surface of glass, mica and platinum, J. Am. Chem. Soc., 40 (1918) 1361–1403.
[32] M.D. Levan, T. Vermeulen, Binary Langmuir and Freundlich isotherms for ideal adsorbed solutions, Phys. Chem., 85 (1981) 3247–3250.
[33] L. Zhang, G. Shi, Preparation of highly conductive graphene hydrogels for fabricating supercapacitors with high rate capability, J. Phys. Chem. C, 115 (2011) 17206–17212.
[34] L.H. Ai, J. Jiang, Removal of methylene blue from aqueous solution with self-assemble cylindrical graphene-carbon nanotube hybrid, Chem. Eng. J., 192 (2012) 156–163.
[35] A.S. El-Azab, Y. Sheena Mary, C.Y. Panicker, A.A.-M. Abdel-Aziz, I.A. Al-Suwaidan, C. Van Alsenoy, FT-IR, FT-Raman and molecular docking study of ethyl 4-(2-(4-oxo-3-phenethyl-3,4-dihydroquinazolin-2-ylthio)acetamido)benzoate, J. Mol. Struct., 1111 (2016) 9–18.
[36] L.L. Jiang, H.T. Yu, X.M. Zhou, X.G. Hou, Z.S. Zou, S.J. Li, C.T. Li, X.Y. Yao, Preparation, characterization and adsorption properties of magnetic multi-walled carbon nanotubes for simultaneous removal of Pb^{2+} and Zn^{2+} from aqueous solutions, Desalin. Water Treat., 57(2016) 18446–18462.
[37] M. Arivazhagan, J.S. Kumar, Vibrational analysis of 4-amino pyrazolo (3,4-d) pyrimidine a joint FTIR, laser Raman and scaled quantum mechanical studies, Spectrochim. Acta, Part A, 82 (2011) 228–234.
[38] P.A.M. Mourao, P.J.M. Carrott, M.M.L. Carrott, Application of different equations to adsorption isotherms of phenolic compounds on activated carbons prepared from cork, Carbon, 44 (2006) 2422–2429.
[39] M. Hadavifar, N. Bahramifar, H. Younesi, Q. Li, Adsorption of mercury ions from synthetic and real wastewater aqueous solution by functionalized multi-walled carbon nanotube with both amino and sulfydrylate groups, Chem. Eng. J., 237 (2014) 217–228.
[40] C. Fernandes, C. Pereira, A. Guedes, S.L.H. Rebelo, C. Freire, Gold nanoparticles decorated on Bingel-sulfydryl functionalized multiwall carbon nanotubes as an efficient and robust catalyst, Appl. Catal., A, 486 (2014) 150–158.
[41] S.S. Nanda, M.J. Kim, K.S. Yeom, S.S. AAn, H. Ju, D.K. Yi, Raman spectrum of graphene with its versatile future perspectives, TrAC, Trends Anal. Chem., 80 (2016) 125–131.
[42] D.W. Wang, K.H. Wu, I.R. Gentle, G.Q. Lu, Anodic chlorine/nitrogen co-doping of reduced graphene oxide films at room temperature, Carbon, 50 (2012) 3333–3341.
[43] M. Barczak, A. Dabrowski, S. Pikus, J. Ryczkowski, P. Borowski, M. Kozak, Studies of the structure and chemistry of SBA-15 organosilicas functionalized with amine, sulfydryl, vinyl and phenyl groups, Appl. Surf. Sci., 256 (2010) 5370–5375.
[44] I.A. Shaaban, A.E. Hassan, A.M. Abuelela, W.M. Zoghaieb, T.A. Mohamed, Infrared, Raman and NMR spectral analysis, vibrational assignments, normal coordinate analysis, and quantum mechanical calculations of 2-amino-5-ethyl-1,3,4-thiadiazole, J. Mol. Struct., 1103 (2016) 70–81.
[45] L.G. Cancado, A. Jorio, E.H.M. Ferreira, F. Stavale, C.A. Achete, R.B. Capaz, Quantifying defects in graphene via Raman spectroscopy at different excitation energies, Nano Lett., 11 (2011) 3190–3196.
[46] S. Rani, M. Kumar, R. Kumar, D. Kumar, S. Sharma, G. Singh, Characterization and dispersibility of improved thermally stable amide functionalized graphene oxide, Mater. Res. Bull., 60 (2014) 143–149.
[47] R. Rostamian, H. Behnejad, A comparative adsorption study of sulfamethoxazole onto graphene and graphene oxide nanosheets through equilibrium, kinetic and thermodynamic modeling, Process Saf. Environ. Prot., 102 (2016) 20–29.
[48] J. Chen, M.G. Zhao, Y.C. Li, J.J. Liang, S.S. Fan, S.G. Chen, Preparation of graphene oxide/multiwalled carbon nanotubes 3D flexible architecture for robust biosensing application, Ceram. Int., 41 (2015) 15241–15245.
[49] D.M. Khan, A. Kausar, S.M. Salman, Buckypapers of polyvinyl chloride/poly(styrene-co-maleic anhydride) blend intercalated graphene oxide-carbon nanotube nanobifiller: physical property exploration, Fullerenes Nanotubes Carbon Nanostruct., 24 (2016) 202–212.
[50] H.Q. Bi, Y.H. Li, S.F. Liu, P.Z. Guo, Z.B. Wei, C.X. Lv, J.Z. Zhang, X.S. Zhao, Carbon-nanotube-modified glassy carbon electrode for simultaneous determination of dopamine, ascorbic acid and uric acid: the effect of functional groups, Sens. Actuators, B, 171 (2012) 1132–1140.
[51] C.M. Babu, R. Vinodh, B. Sundaravel, A. Abidov, M.M. Peng, W.S. Cha, H.T. Jang, Characterization of reduced graphene oxide supported mesoporous Fe_2O_3/TiO_2 nanoparticles and adsorption of As(III) and As(V) from potable water, J. Taiwan Inst. Chem. Eng., 62 (2016) 199–208.
[52] G.D. Vukovic, A.D. Marinkovic, M. Colic, M.D. Ristic, R. Aleksic, A.A. Peric-Grujic, P.S. Uskokovic, Removal of cadmium from aqueous solutions by oxidized and ethylenediamine-functionalized multi-walled carbon nanotubes, Chem. Eng. J., 157 (2010) 238–248.
[53] L.H. Jiang, Y.G. Liu, G.M. Zeng, F.Y. Xiao, X.J. Hu, X. Hu, H. Wang, T.T. Li, L. Zhou, X.F. Tan, Removal of 17β-estradiol by few-layered graphene oxide nanosheets from aqueous solution: external influence and adsorption mechanism, Chem. Eng. J., 284 (2016) 93–102.
[54] J.C. Lazo-Cannata, A. Nieto-Marquez, A. Jacoby, Adsorption of phenol and nitrophenols by carbon nanospheres: effect of pH and ionic strength, Sep. Purif. Technol., 80 (2011) 217–224.
[55] Y.B. Sun, S.B. Yang, Y. Chen, C.C. Ding, W.C. Cheng, X.K. Wang, Adsorption and desorption of U(VI) on functionalized graphene oxide a combined experimental and theoretical study, Environ. Sci. Technol., 49 (2015) 4255–4262.
[56] H.A. Mengistu, A. Tessema, M.B. Demlie, T.A. Abiye, O. Roeyset, Surface-complexation modelling for describing adsorption of phosphate on hydrous ferric oxide surface, Water SA, 41 (2015) 157–167.
[57] G.P. Rao, C. Lu, F. Su, Sorption of divalent metal ions from aqueous solution by carbon nanotubes: a review, Sep. Purif. Technol., 58 (2007) 224–231.
[58] X.X. Wang, Z.S. Chen, X.K. Wang, Graphene oxide for simultaneous highly efficient removal of trace level radionoclides from aqueous solution, Sci. Chin. Chem., 58 (2015) 1766–1773.
[59] I.A. Tan, A.L. Ahmad, B.H. Hameed, Adsorption of basic dye on high-surface-area activated carbon prepared from coconut husk: equilibrium, kinetic and thermodynamic studies, J. Hazard. Mater., 154 (2008) 337–346.
[60] K.Y. Foo, B.H. Hameed, Insights into the modeling of adsorption isotherm systems, Chem. Eng. J., 156 (2010) 2–10.
[61] Q. Hu, Z. Xiao, X. Xiong, G. Zhou, X. Guan, Predicting heavy metals' adsorption edges and adsorption isotherm on MnO with the parameters determined from Langmuir kinetics, J. Environ. Sci., 27 (2015) 207–216.
[62] H. Al-Gohani, M.A. Salam, Kinetics and thermodynamics study of aniline adsorption by multiwalled carbon nanotubes from aqueous solution, J. Colloid Interface Sci., 360 (2011) 760–767.
[63] X.D. Ren, Z.H. Xiong, Magnetic multi-walled carbon nanotubes on the water adsorption behavior of three kinds of nitro imidazoles drugs, Acta Chim. Sinica, 71 (2013) 625–633.
[64] I. Mobasherpour, E. Salahi, M. Ebrahimi, Thermodynamics and kinetics of adsorption of Cu(II) from aqueous solutions onto multi-walled carbon nanotubes, J. Saudi Chem. Soc., 18 (2014) 792–801.